Enhancement of TiO₂ Photocatalyst Using Rare Earth Oxide (La₂O₃) via a Simple Preparation Method for Degradation of Methylene Blue under Visible Light

Taufik Abdillah Natsir*, Alam Reformasi Putra Pamungkas, Nurul Hidayat Aprilita

Department of Chemistry, Universitas Gadjah Mada, Sekip Utara, Bulaksumur, Yogyakarta 55281 Indonesia

*Corresponding author email: taufik.abdillah@ugm.ac.id

ABSTRACT. The modification of TiO₂ using rare earth oxide (La₂O₃) to increase the photodegradation activity of TiO₂ under visible light has been conducted. The goal of this research is to identify the influence of La₂O₃ on the TiO₂ to the photocatalytic activity of TiO₂. The mixed oxide of TiO₂/La₂O₃ was prepared using the precipitation method. The as-prepared catalyst was then calcined at 923 K. The photocatalyst was characterized using SRUV, XRD, FTIR, and SEM-EDX. The results showed that the photocatalyst activity of TiO₂/La₂O₃-923 under visible light in the degradation of methylene blue was higher than pristine TiO₂. The decrease in bandgap energy of TiO₂/La₂O₃-923 from 3.2 eV to 3.01 eV was not the main factor in the increase of photocatalytic activity of TiO₂/La₂O₃-923. The optimum condition of photodegradation of MB was obtained when the ratio of TiO₂/La₂O₃ was 5, the concentration of MB was 10 ppm, the reaction time was 300 min, and the mass of the photocatalyst was 0.25 g. The reusability of TiO₂/La₂O₃-923 was stable up to 3 sequent runs with the MB photodegradation of more than 90%. The mechanistic study of the mixed oxide TiO₂/La₂O₃ showed that the hydroxyl radical played an important role in its high photocatalytic.

Keywords: TiO₂-La₂O₃, photocatalyst, visible light, methylene blue

INTRODUCTION

Recently, the global industrial sector has been growing rapidly, primarily driven by economic factors. Countries are striving to boost their income to enhance the well-being of their citizens. However, this growth in the industrial sector has also been a significant contributor to environmental issues. The untreated waste generated by industries, such as wastewater, can harm the environment. Consequently, the development of wastewater treatment methods within the industrial sector has garnered significant attention from researchers.

Various research on wastewater treatment have been conducted, such as biological, physical, chemical methods including adsorption, coagulation, sonolysis, electrodegradation, and photocatalyst (Alexander et al., 2012; Awad et al., 2019; Lan et al., 2013; Wang et al., 2009). However, photocatalysts attract more attention because they use solar light to degrade organic pollutants. Some metal oxides exhibit photocatalytic activity, and TiO₂ has been proven to be an effective heterogeneous catalyst in various photocatalytic applications, including soil purification, air purification, water purification, and self-cleaning. (Lan et al., 2013) Semiconductor TiO₂ shows superiority in photocatalytic activity and has other advantages such as its high stability, cheap, non-toxic, and abundant. However, its photocatalytic activity was restricted only in UV radiation in which solar radiation contains only 2 – 4% of UV light due to high band gap energy (3.0 – 3.2 eV) and fast recombination. (Yu et al., 2015) Therefore, the modification of TiO₂ to increase its photocatalytic activity in visible light is needed. Several methods have been developed to increase the photocatalytic activity of TiO₂, such as doping elements, noble metal deposition, inorganic acid modification, dye sensitization, metal ion implantation, and heterojunction (Humayun et al., 2018). The addition of rare earth elements to TiO₂ has garnered attention from researchers due to their 4f orbital configuration, which can significantly enhance the photocatalytic activity of TiO₂ (Liang et al., 2008; Wu et al., 2010). The addition of lanthanum to TiO₂ in photocatalytic activity has been investigated by several researchers (Azam et al., 2019; Li & Feng, 2016; Wang et al., 2016; Zhang et al., 2014). However, their studies focused on catalytic activity and its preparation. To the best of our knowledge, a detailed investigation into the mechanism of this material has not yet been conducted. In this research, we focused on the study of mechanistic study.

EXPERIMENTAL SECTION
Materials
The following materials were used to synthesize the catalyst: commercial TiO₂, commercial La₂O₃, HNO₃

65%, and NaOH. All materials were obtained from Merck. Methylene blue, Benzoquinone, 2-propanol, and ethylenediaminetetraacetic acid (EDTA) were purchased from Merck.

Preparation of The Catalyst

The catalyst (TiO₂/La₂O₃) was prepared using a typical procedure. A certain amount of commercial La₂O₃ was dissolved in 1.5 mL of HNO₃ 65%, then diluted using distilled water to 41 mL. Titanium dioxide (TiO₂) was added to the solution. The mole ratio of TiO₂ to La₂O₃ was set at 1, 2, 5, and 10. After mixing, 3 M aqueous NaOH was added to the solution until the pH reached 12. The precipitated was filtered and dried at 383 K and denoted as TiO₂/La₂O₃ (x). The as-prepared catalyst was then calcined at 923 K for 2 hours and denoted as TiO₂/La₂O₃-923 (x), where x is the mol ratio of TiO₂ to La₂O₃. As a control, a commercial TiO₂ was treated as a previous method without the presence of La₂O₃. The control was denoted as TiO₂-923. The catalyst was characterized using FTIR, SEM-EDX, SRUV, and XRD.

FTIR Experiment

A pellet was prepared by mixing a certain amount of sample and KBr. Fourier transform infrared (FTIR) spectra were recorded on Shimadzu IR Prestige-21 spectrophotometer in the range 400 – 4000 cm^{-1}.

XRD Experiment

The powder X-ray diffraction pattern of the samples was recorded on Shimadzu ZRD 6000. Scans were conducted over a 2θ range from 10° to 80°. The crystallite size of TiO₂ was calculated using the Scherrer equation for the crystal planes (101) and (200), and the lattice parameters were calculated using the following equations (Lin & Yu, 1998)

$$D = \frac{0.89\lambda}{\beta cos\theta}$$

$$d_{(hkl)}^{-2} = h^2a^{-2} + k^2b^{-2} + l^2c^{-2}$$

where, D= is the measure of crystal size, λ is the wavelength of X-ray radiation (1540 nm), β is the full width at half maximum, and θ represents the diffraction angle.

SEM-EDX Experiment

The sample was dehydrated to minimize its interference. The images of the samples were recorded using a Scanning Electron Microscope (SEM) Hitachi SU 3500. The element analysis of the samples was determined using EDAX Element.

Specular Reflectance UV-Vis Experiment

An amount of samples was compacted to make a pellet. The absorbance of samples was recorded using *Specular Reflectance* UV-Vis (Pharmaspec UV 1700). The Bandgap energy was calculated from band-edge absorption (λ$_g$) using the following equation (Cao et al., 2010):

$$Eg(eV) = {1240}/{\lambda_g(nm)}$$

Photocatalytic Activity

Briefly, in a typical experiment, 50 mL of methylene blue (MB) with a certain concentration was put into a container. The catalyst (0.1 g) was added to the solution. The mixture was placed into the reactor and illuminated by visible (Hannoch lamp 530-590 nm), UV-Vis lamp (Philips UV lamp 254 nm), or solar radiation (at 10.00-12.00 am) for a desired time. As a control, the other mixture was put into the dark. After that, the solution was separated by using a centrifuge at 5800 rpm for 30-60 minutes. The rest of the MB in the solution was analyzed using a UV-Vis Spectrophotometer at a wavelength of 665 nm.

RESULTS AND DISCUSSION
The Photocatalytic Performance of TiO₂/La₂O₃

First, the photodegradation of MB was conducted under various photocatalysts, i.e., TiO₂-923, La₂O₃-923, and TiO₂/La₂O₃-923(5) as shown in **Figure 1**. The photodegradation of MB using TiO₂-923 shows high catalytic activity under solar radiation and UV light up to 96%. On the contrary, the activity of TiO₂-923 under visible light decreased up to 43% removal of MB. It seems that the treatment of TiO₂ under high temperatures influenced the activity of TiO₂ under solar radiation since solar radiation contains visible light about 44 – 46% of the incoming radiation (Malato et al., 2009; Wu et al., 2014). Meanwhile, La₂O₃ shows low activity in photodegradation under all the tested conditions due to a high band gap energy of about 5.5 eV (Zhang et al. 2019). The addition of La₂O₃ to TiO₂ significantly increased the activity of TiO₂ in the removal of MB under visible light, achieving up to a 94% removal rate. The activity of the TiO₂/La₂O₃ under dark confirmed that the removal of MB was not influenced by a photocatalytic activity but by an adsorption process (**Figure 1**). However, the adsorption of MB on the catalyst surface increased after the addition of La₂O₃ to TiO₂. This result is consistent with other research that La₂O₃ enhanced the adsorption of dye compounds such as congo red (Moothedan & Sherly, 2016). In photocatalytic activity, the adsorption of a compound on the catalyst surface is crucial (Humayun et al., 2018). Therefore, the enhancement of MB adsorption on the photocatalyst can be achieved through the modulation of co-dopants, such as La₂O₃. In addition to the adsorption process, it is necessary to investigate the bandgap energy of these catalysts because a low bandgap energy represents increased photocatalytic activity under lower wavelengths.

The bandgap energy of the TiO₂, TiO₂-923, and TiO₂/La₂O₃-923 (5) was investigated using UV reflection as shown in **Figure 2**. These samples have subtle differences in absorption edge locations at 387, 409, and 411 nm, respectively. The band gap of the catalysts was calculated from their absorption edge according to the reference (Cao et al., 2010), and was found that the bandgap of TiO₂, TiO₂-923, and

TiO_2/La_2O_3-923 was estimated to be about 3.2, 3.05, and 3.08 eV, respectively as shown in **Table 1**. The calcination of TiO_2 under 923 K shows a lower bandgap (entry 3) than pristine TiO_2 (entry 1). This result means that the bandgap of TiO_2 can be decreased by treating it at high temperatures (Wu et al., 2014). The treatment of TiO_2 under high temperatures causes form oxygen vacancy that causes ion Ti^{4+} to be reduced to Ti^{3+} (Wu et al., 2010). The formation of Ti^{3+} can be an electron trap to retard the recombination process (Aronne et al., 2017; Wu et al., 2010). However, the photodegradation of both catalysts i.e. pristine TiO_2 and TiO_2-923 showed the same result under visible light (**Figure 1**) indicating the oxygen vacancy was not effective to retard the recombination process. Meanwhile, the TiO_2/La_2O_3-923 (5) (entry 2) has a similar bandgap energy with TiO_2-923 (entry 3), but the photocatalytic activity of TiO_2/La_2O_3-923 (5) under visible light is higher than TiO_2-923 as shown in **Figure 1**. Therefore, the bandgap energy is not the main factor why the addition of La_2O_3 on the TiO_2 is active under visible. A thorough investigation of all the tested photocatalysts is required.
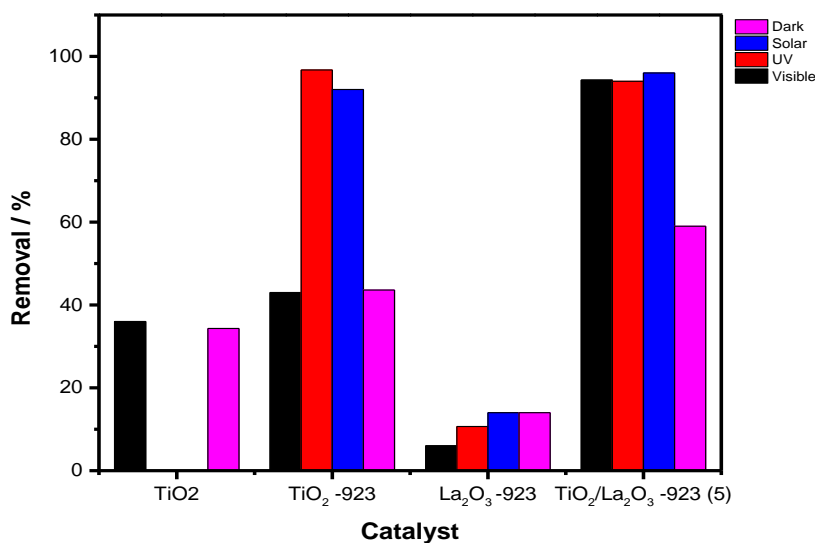

Figure 1. Photodegradation of MB under various catalysts. (Reaction condition: MB = 1.5 ppm, catalyst = 0.1 g, t = 1 h, pH = 6.7)
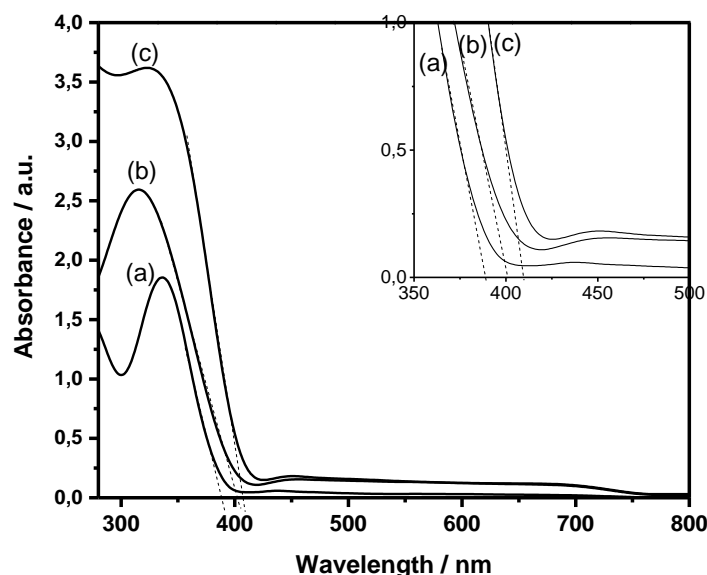

Figure 2. The UV reflection of tested catalysts (**a**) TiO_2, (**b**) TiO_2/La_2O_3-923, and (**c**) TiO_2-923.

Table 1. The bandgap energy of photocatalyst

Entry	Material	Wavelength /nm	Bandgap energy / eV
1	TiO_2	387	3.20
2	TiO_2/La_2O_3-923 (5)	403	3.08
3	TiO_2-923	406	3.05

The high photocatalytic performance of TiO$_2$/La$_2$O$_3$ under visible light probably occurs because La^{3+} ions replace Ti lattice ions at its interface. The alteration of the TiO$_2$ lattice due to the dopant could influence the photocatalytic properties of TiO$_2$ (McManamon et al., 2015). The XRD experiment was conducted and the diffractogram profile of the tested catalysts is shown in **Figure 3**. The TiO$_2$ calcined at 923 K shows the same pattern as pristine TiO$_2$. The dominant phase of TiO$_2$ was anatase. The peak at 22.4° was also detected as Ti$_6$O$_{11}$.(Le Page & Strobel, 1983) It indicated that the treatment of TiO$_2$ under high temperatures at 923 K did not change the crystallinity of TiO$_2$ from anatase to rutile. This result is in contrast with the other researchers who that reported the rutile phase was formed when TiO$_2$ was treated under a high temperature of more than 773 K (Wu et al., 2014). The difference in the result is probably due to the duration of calcination. The crystallite size of calcined TiO$_2$ is slightly higher than pristine TiO$_2$, i.e., 40 nm and 37 nm, respectively. This result is in accordance with the other report that the effect of crystallite size of metal oxide was influenced by the calcination temperature (Natsir et al., 2018).

The addition of lanthanum does not change the crystallinity of TiO$_2$. Lanthanum hydroxide, La(OH)$_3$ phase was detected before TiO$_2$/La$_2$O$_3$ was calcined. The La$_2$O$_3$ phase was formed after the catalyst was treated at 923 K. The crystallite size of calcined TiO$_2$/La$_2$O$_3$ is lower than TiO$_2$-923, i.e. 21 nm and 40 nm, respectively indicating that La$_2$O$_3$ inhibits the agglomeration of TiO$_2$ due to the presence of Ti-O-La bond at its interface (Li & Feng, 2016). The lattice parameter of TiO$_2$/La$_2$O$_3$ showed that there is no different lattice value with TiO$_2$-923 indicating La^{3+} was not intercalated into the TiO$_2$ lattice. The crystal ionic radius of La^{3+} size is higher than Ti^{4+} i.e., 0.155

nm and 0.068 nm, respectively (Wang et al., 2016). Therefore at the TiO$_2$/La$_2$O$_3$ mole ratio prescribed, i.e., TiO$_2$/La$_2$O$_3$ mole ratio was 5, La^{3+} does not change the TiO$_2$ lattice and La$_2$O$_3$ was placed on the TiO$_2$ surface.

The FTIR spectra revealed the functional groups of the tested photocatalysts surface as shown in **Figure 4**. The IR spectra of TiO$_2$-923 and TiO$_2$/La$_2$O$_3$-923 (5) showed a similar pattern. However, TiO$_2$/La$_2$O$_3$-923 (5) showed a different peak at 975 cm^{-1}. There are two possibilities to explain this peak that is the up-conversion process occurred or the Ti^{4+} intercalated into the La$_2$O$_3$ lattice at its interface to form La – O – Ti (Obregón & Colón, 2012; Wu et al., 2010).

To identify the peaks associated with the up-conversion process, photodegradation experiments were conducted under IR light. The degradation of TiO$_2$/La$_2$O$_3$-923 (5) under IR light was slightly higher than under dark (**Figure 5(a)**). This result showed that the up-conversion process seemingly occurred. However, the temperature of the solution slightly increased after the IR light was used, i.e. up to 333 K. The degradation of MB under high temperature i.e., at 333 K showed the same result under IR light (**Figure 5(b)**). The high activity of photocatalysts at high temperatures occurs due to the increase in kinetic energy (Bai et al., 2020). Therefore, we conclude that the up-conversion process of TiO$_2$/La$_2$O$_3$-923 (5) did not proceed, but the intercalation of Ti^{4+} in the interface of the La$_2$O$_3$ lattice occurred. The intercalation of Ti^{4+} to replace the La^{3+} ion occurred in the interface between TiO$_2$ and La$_2$O$_3$ creating an imbalance charge that will be neutralized by hydroxides on the surface (Xu et al., 2002). The presence of OH could be detected by FTIR at 975 cm^{-1} as the vibration of La-OH (Kustov et al., 1981).
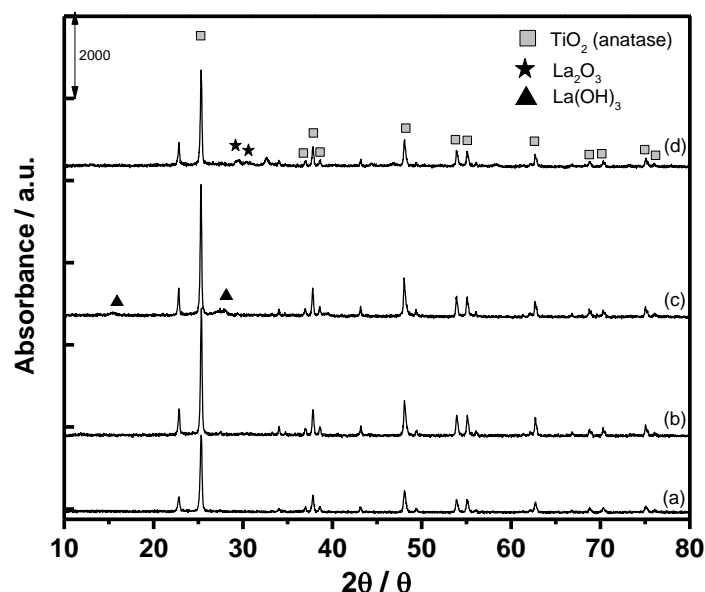

Figure 3. Diffractogram pattern of (**a**) pristine TiO$_2$, (**b**) TiO$_2$-923, (**c**) TiO$_2$/La$_2$O$_3$ (5), (**d**) TiO$_2$/La$_2$O$_3$-923 (5)

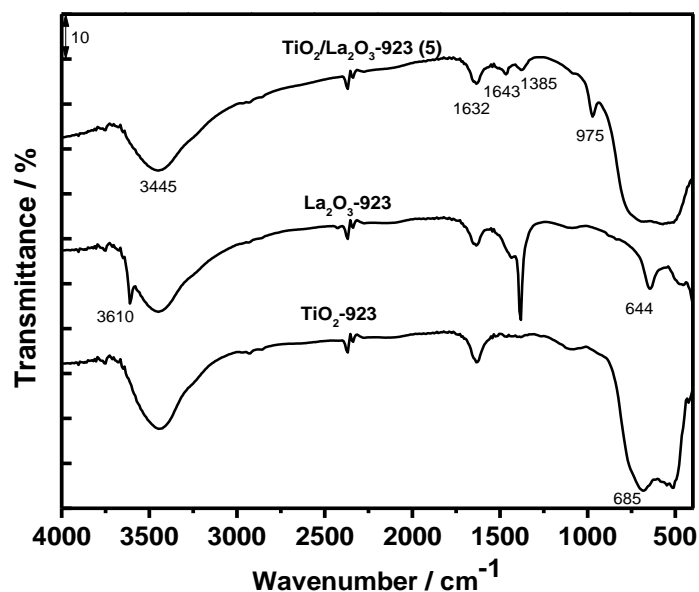Figure 4. The FTIR spectra of TiO_2-923, TiO2-923 and TiO_2/La_2O_3-923 (5)

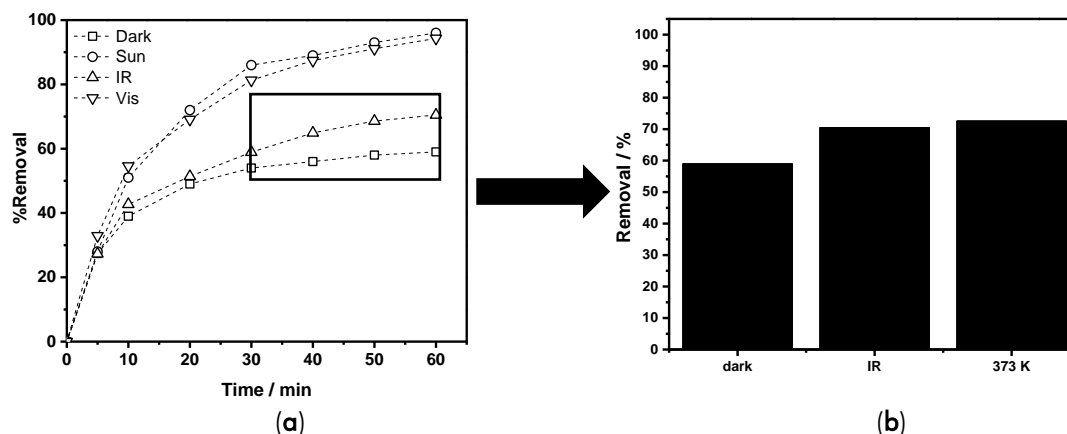

Figure 5. The % removal of MB under different (a) times and (b) under temperature at 333 K. reaction condition: MB = 1.5 ppm, catalyst = 0.1 g, t = 1 h, pH = 6.7

The effectiveness of reaction conditions in the photodegradation of TiO_2/La_2O_3 was also investigated, such as pH, catalyst amount, and MB concentration. As shown in Figure 6(a), the optimum pH was achieved at 6.7. At low pH, the catalyst surface was protonated causing the MB to be hindered to attach on the catalyst surface. Meanwhile, at pH more than the optimum condition, the catalyst surface and OH compete to interact with MB, thereby resulting in a decreased adsorption of MB (Pathania et al., 2017). The optimum catalyst mass was achieved at 0.25 gram/50 mL solution as shown in **Figure 6(b)**. The excess of catalyst mass caused the penetration of light to be disturbed resulting the low photocatalytic activity. Meanwhile, the low amount of catalyst is inadequate to maximize the photodegradation process (Herrmann, 2005; Malato et al., 2009). The higher initial concentration of MB shows a lower photodegradation process than the low concentration of MB as shown in **Figure 6(c)**. The high initial concentration of MB causes the catalyst to be covered by adsorbate and reduces the penetration of light to the photocatalyst, thus the photodegradation decreases (Herrmann, 2005). However, when the reaction time was prolonged at the high initial concentration of MB, i.e. 10 ppm, the photodegradation of TiO_2/La_2O_3 showed a high catalytic performance as shown in **Figure 6(d)**.

The stability of the photocatalyst was also studied as shown in **Figure 7**. The TiO_2/La_2O_3-923 (5) showed high stability in the photodegradation until 3 runs. The high stability of the catalyst was analyzed using FTIR and XRD. The FTIR result of the fresh and used catalysts showed no difference in the spectra. In addition, the diffractogram of the used catalyst did not show new peaks. Lanthanum oxide (La_2O_3) is hygroscopic in nature and easy to convert to $La(OH)_3$ when reacts with water (Fleming et al., 2010). The composite of TiO_2/La_2O_3 was able to maintain the La_2O_3 phase on the catalyst surface even though the reaction was conducted in water as a solvent.
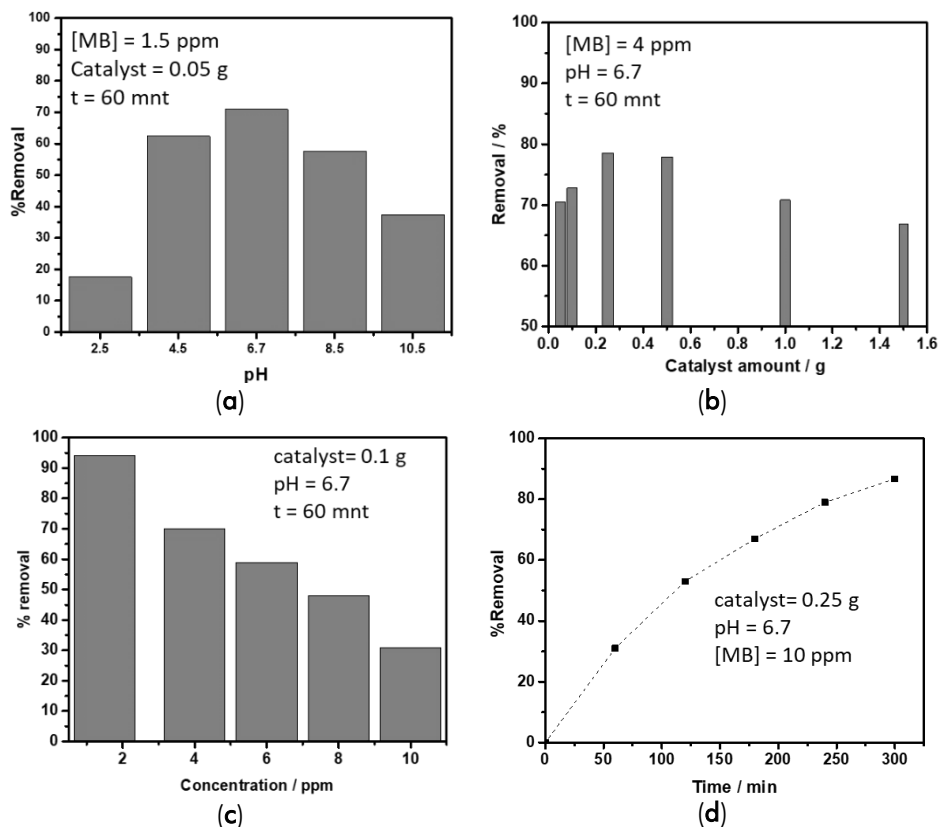
Figure 6. Photodegradation of TiO_2/La_2O_3-923 (5) under visible light at various (**a**) pH, (**b**) mass of catalyst, (**c**) initial concentration of MB, and (**d**) time profile.
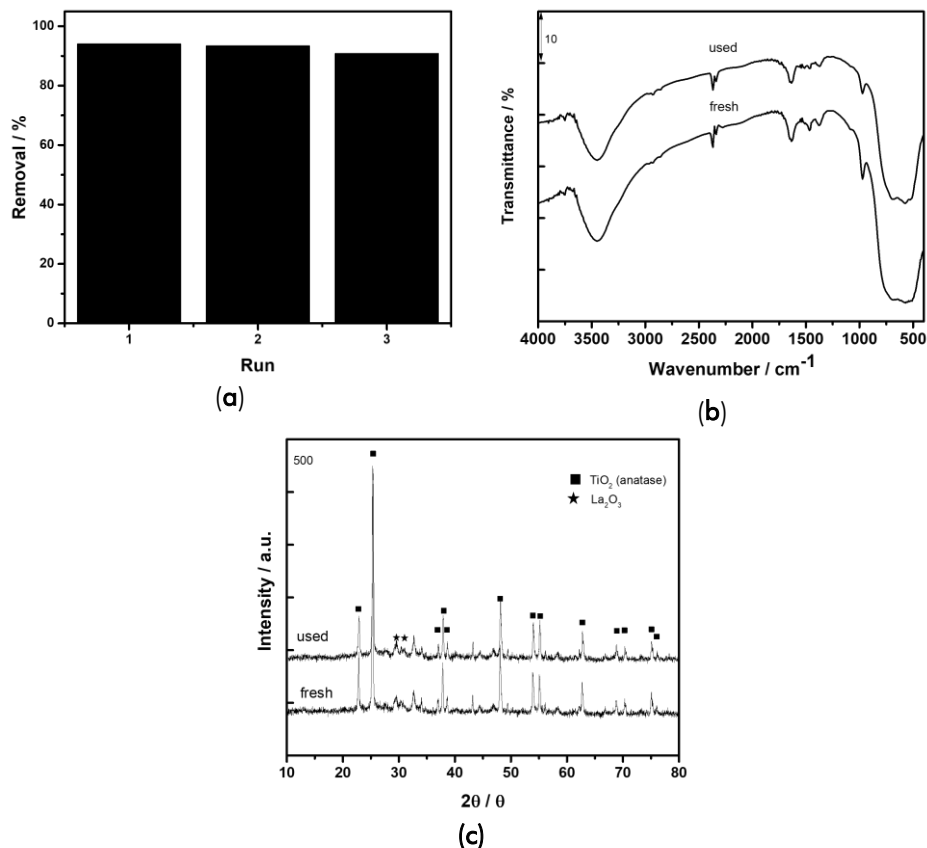

Figure 7. (**a**) The photocatalytic performance of TiO_2/La_2O_3-923 (5) up to 3 runs, (**b**) FTIR spectra, and (**c**) diffractogram of fresh and used photocatalyst.

The Effect of La³⁺ on The Photocatalyst.

The effect of La^{3+} on the TiO_2 was also studied under different mole ratios, as shown in **Table 2**. The lattice parameter of photocatalyst was determined from the diffractogram of crystal planes (101) and (200) as shown in **Table 3** (Lin & Yu, 1998). The addition of La^{3+} on the TiO_2 without calcination seemingly did not influence the lattice parameters of TiO_2 as shown in **Table 3** (entry 7). The La_2O_3 presence on the surface of TiO_2. The heat treatment of La_2O_3/TiO_2 at a high temperature (623 K) affected the lattice parameter of TiO_2. The cell parameter "c" of TiO_2 increases after it was modified with La_2O_3 and treated at high temperature indicating the La^{3+} incorporated into the TiO_2 lattice at its interface, except for TiO_2/La_2O_3 (5). This result has been consistent with the previous result showing that the incorporation of metal into the TiO_2 was influenced by high temperature (Colón et al., 2002). The lattice parameter TiO_2/La_2O_3-923 (5) is similar to pristine TiO_2 indicating those optimum molar ratios were achieved. The incorporation of La^{3+} into the TiO_2 lattice at its interface is corroborated by the change in the diffractogram intensity of TiO_2/La_2O_3-923 (1, 2, and 10) as shown in **Figure 7** that indicates the structure of TiO_2 is perturbated.

The crystallite size of TiO_2/La_2O_3-923 (x) is smaller than TiO_2 indicating the presence of a Ti-O-La bond at the interface of the composite (Li & Feng, 2016).

The photocatalysts of all TiO_2/La_2O_3-923 (x) (**Table 3**, entries 1 to 4) showed higher photocatalytic activity than TiO_2-923 (entry 5). The addition of La^{3+}, i.e. the molar ratio of TiO_2 to La_2O_3 from 10 to 5, increased the photocatalytic activity up to 94%. The addition of La^{3+} more than the optimum condition, i.e. molar ratio of TiO_2 to La_2O_3 up to 1 decreased its photocatalytic activity due to the presence of $La(OH)_3$ on the TiO_2 surface as shown in **Figure 8**. The band gap energy of various TiO_2/La_2O_3 is relatively similar as shown in **Table 3**. The result indicates that the band gap energy is not the main reason why the addition of La^{3+} enhances the photocatalytic of TiO_2. The addition of La on the TiO_2 increases the adsorption of MB that facilitates to transfer of radical species from the photocatalyst surface to the adsorbate or can act as an efficient separator of photoexcited electron and hole as previously discussed (Li & Feng, 2016; Liang et al., 2008; Ranjit et al., 2001; Xu et al., 2002; Xu et al., 2010). In addition, the addition of La on the TiO_2 surface inhibits the recombination process (Husna et al., 2023).

Table 2. Lattice parameters Comparison of various TiO_2/La_2O_3

Entry	Photocatalyst	a=b (Å)	c (Å)	Cell volume (Å³)	Crystallite size* (nm)
1	TiO_2/La_2O_3-923 (1)	3.73	10.60	147.92	21
2	TiO_2/La_2O_3-923 (2)	3.79	9.68	138.95	21
3	TiO_2/La_2O_3-923 (5)	3.78	9.52	136.17	21
4	TiO_2/La_2O_3-923 (10)	3.79	9.83	141.53	20
5	TiO_2-923	3.78	9.44	135.17	40
6	TiO_2	3.78	9.52	136.17	37
7	TiO_2/La_2O_3-(5)	3.78	9.47	135.71	58

*Crystallite size was determined using the Scherrer equation at crystal pane (101).
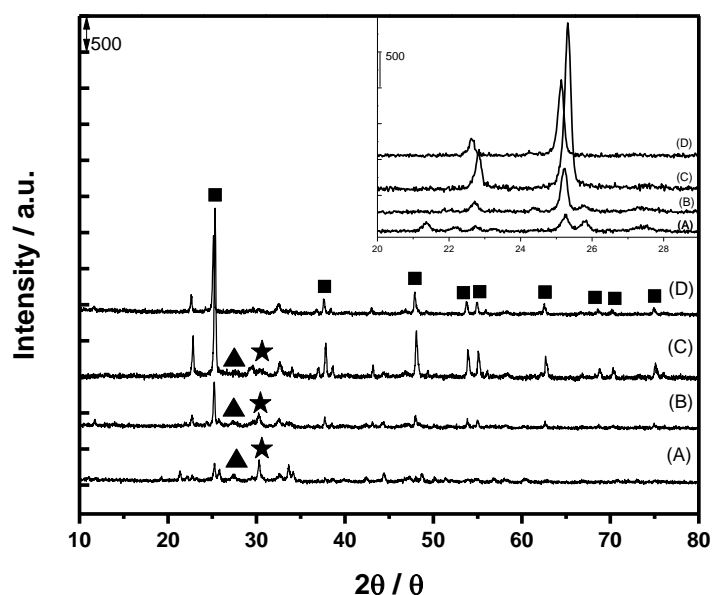
Figure 8. The diffractogram of various mole ratios of (A) TiO_2/La_2O_3-923 (1), (B) TiO_2/La_2O_3-923 (2), (C) TiO_2/La_2O_3-923 (5), and (D) TiO_2/La_2O_3-923 (10). Note: ■ = TiO_2, ▲ = $La(OH)_3$, ★ = La_2O_3.

Table 3. Comparison of various TiO$_2$/La$_2$O$_3$ in the UV reflectance properties and the photocatalytic activity

Entry	Photocatalyst	band-edge absorption (nm)[1]	Bandgap energy[1] (eV)	%Removal[2]
1	TiO$_2$/La$_2$O$_3$-923 (1)	400	3.10	57.1
2	TiO$_2$/La$_2$O$_3$-923 (2)	411	3.01	78.4
3	TiO$_2$/La$_2$O$_3$-923 (5)	400	3.10	94.3
4	TiO$_2$/La$_2$O$_3$-923 (10)	392	3.16	76.4
5	TiO$_2$-923	409	3.03	43.0

[1]Bandgap energy was calculated using (Cao et al., 2010): $Eg(eV) = {1240}/{\lambda_g(nm)}$.

[2]Reaction condition: MB = 1.5 ppm, catalyst = 0.1 g, t = 1 h, pH = 6.7, under visible light.
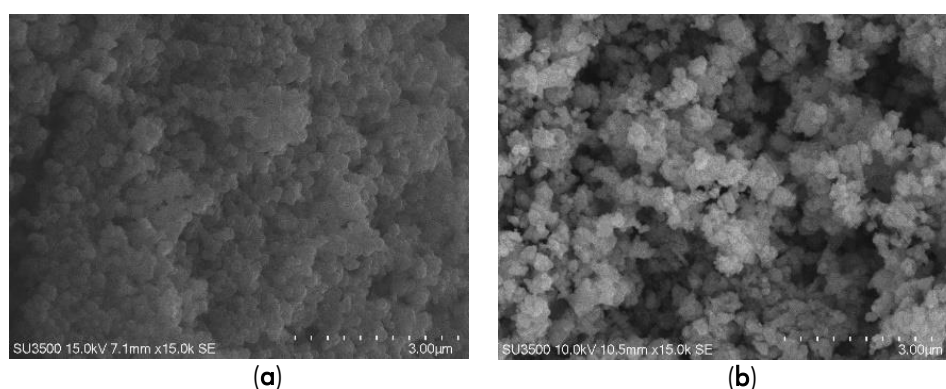
Figure 9. Morphology image of (a) TiO$_2$ and (b) TiO$_2$/La$_2$O3-923 (5)

The morphology of TiO$_2$/La$_2$O$_3$ was analyzed using SEM-EDX as shown in **Figure 9**. The SEM image of TiO$_2$/La$_2$O$_3$-923 (5) shows that its surface seems rougher than pristine TiO$_2$ (**Figure 9(a)**) indicating the La$_2$O$_3$ presence on the surface of TiO$_2$. The shape of the TiO$_2$ particle is almost rectangular-like and about 292 ± 73 nm in length as shown in **Figure 9(b)**. The molar TiO$_2$ and La$_2$O$_3$ were 69.7% and 3.2%, respectively. This result is in accordance with the total amount of TiO$_2$ and La$_2$O$_3$ that was used to prepare the photocatalyst.

Mechanism Study

The mechanism study of TiO$_2$/La$_2$O$_3$ was studied using various radical scavengers such as benzoquinone, isopropyl alcohol, and EDTA to interact with superoxide radical ($^\bullet$O$_2^-$), hydroxyl radical ($^\bullet$OH), and hole in the valency band, respectively (Liu et al., 2017). The addition of radical scavengers to the solution significantly reduced the photocatalytic activity of TiO$_2$/La$_2$O$_3$ as shown in **Figure 10**. The addition of isopropyl alcohol to the solution showed the highest decrease in the photocatalytic activity of TiO$_2$/La$_2$O$_3$ indicating that radical hydroxide was the main species radical in the solution. Meanwhile, the addition of EDTA did not show a significant decrease in the photocatalytic performance indicating the recombination process was not proceeded. This result is consistent with the FTIR study, which suggests that the presence of hydroxides on the catalyst surface plays a significant role in the photocatalytic

performance of TiO$_2$/La$_2$O$_3$. The other researcher also reported that the hydroxyl ion (OH$^-$) combine with the hole of the valence band to form hydroxyl radicals ($^\bullet$OH) and retarded the recombination process (Zhu et al., 2018). In addition, the intercalation of Ti^{4+} to La$_2$O$_3$ lattice, La^{3+}, and the oxygen vacancy trap electrons to inhibit the recombination process (Wu et al., 2010; Xu et al., 2002).

The plausible mechanism of photodegradation of TiO$_2$/La$_2$O$_3$-923 (5) under visible light is shown in **Figure 11**. According to the previous discussion, the preparation of photocatalysts under high temperatures (923 K) facilitated the surface oxygen vacancy. The presence of oxygen vacancy and the intercalation of Ti^{4+} to the La$_2$O$_3$ lattice caused to reduction of Ti^{4+} to Ti^{3+} on the catalyst surface (Wu et al., 2010). The imbalance of those charges on the catalyst surface is stabilized by the presence of hydroxyls on the surface. These hydroxyls can interact with holes generated by visible light irradiation to form hydroxyl radicals ($^\bullet$OH) that then oxidize adsorbed MB. In addition, Ti^{3+} on the surface is not stable and releases electrons that react with adsorbed oxygen to produce superoxide radicals ($^\bullet$O$_2^-$). The formed superoxide radicals ($^\bullet$O$_2^-$) in part react with adsorbed MB, and the rest of these radicals react with proton (H$^+$) to form hydrogen superoxide radical ($^\bullet$HO$_2$). Then, the hydrogen superoxide radical ($^\bullet$HO$_2$) reacts with H$^+$ to form hydrogen peroxide that finally produces hydroxyl radicals ($^\bullet$OH). The formation of $^\bullet$OH can be seen in the following reaction.
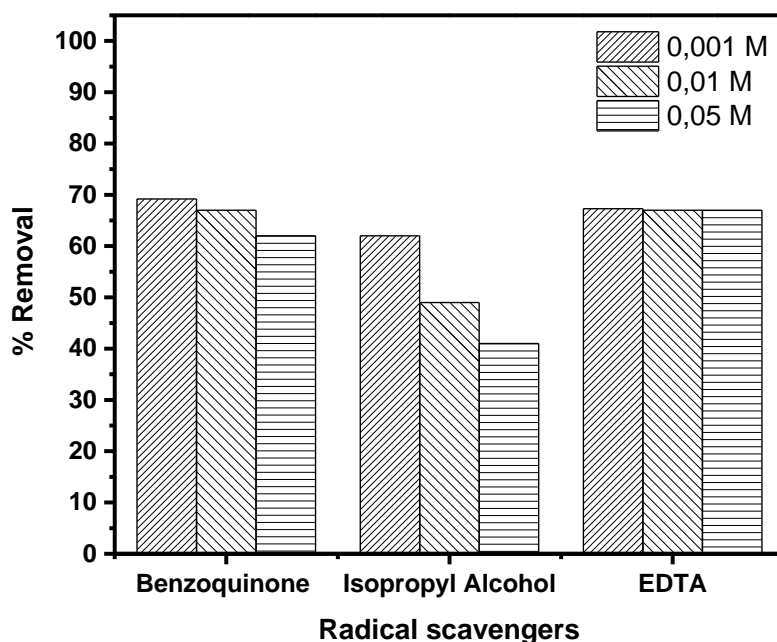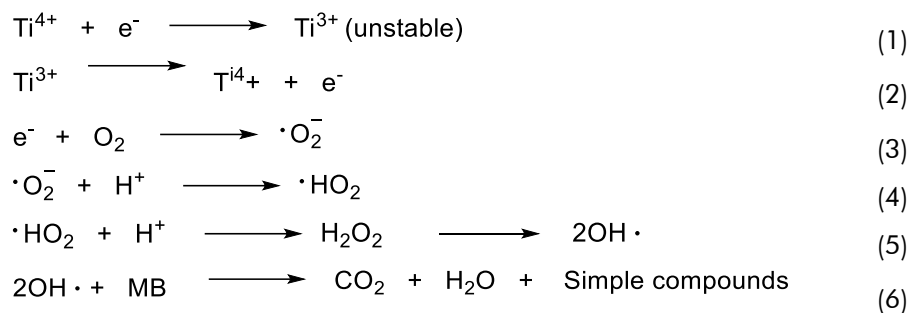
$$Ti^{4+} + e^- \longrightarrow Ti^{3+} \text{ (unstable)} \tag{1}$$

$$Ti^{3+} \longrightarrow Ti^{4+} + e^- \tag{2}$$

$$e^- + O_2 \longrightarrow {}^{\bullet}O_2^- \tag{3}$$

$${}^{\bullet}O_2^- + H^+ \longrightarrow {}^{\bullet}HO_2 \tag{4}$$

$${}^{\bullet}HO_2 + H^+ \longrightarrow H_2O_2 \longrightarrow 2OH^{\bullet} \tag{5}$$

$$2OH^{\bullet} + MB \longrightarrow CO_2 + H_2O + \text{ Simple compounds} \tag{6}$$

Figure 10. Photocatalytic activity of TiO_2/La_2O_3-923 (5) after the addition of radical scavengers
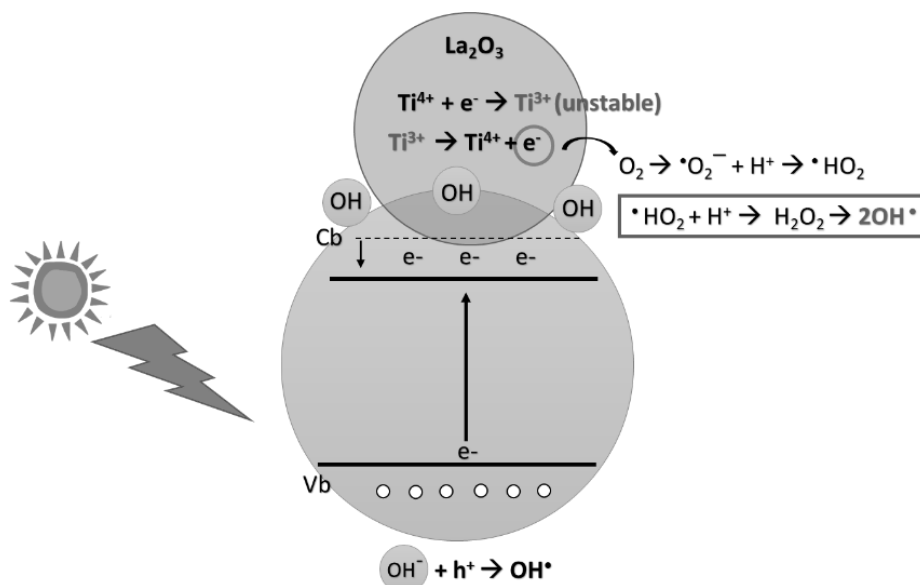

Figure 11. Plausibel mechanism of TiO_2/La_2O_3-923 (5)

According to the information in **Table 4**, La_2O_3/TiO_2 photocatalysts degraded methylene blue under visible light by 87% with a concentration of 10 ppm for 300 min and a mass of 0.25 g photocatalysts. This result is still comparable with the other researchers. Combining rare earth oxides with TiO_2 resulted in higher photocatalytic activity compared to using a single rare earth oxide. Therefore, compared to other materials, this photocatalyst material offers benefits to degrade MB in the wastewater.

Table 4 Comparison result

Catalyst	Adsorbate	Condition	Reference
Y/Eu-TiO$_2$	Methylene Blue	UV; 20 ppm; 2 g; 2 h; 86%	(Wang et al., 2015)
TiO$_2$- coated glass flat membrane	Methylene Blue	UV; 20 ppm; 2 g; 4 h; 90%	(Tan et al., 2023)
Ba/Sr-La	Methylene Blue	UV; 5 ppm; 0,02 g; 65 min; 89,92%	(Ata et al., 2023)
Ni/Fe$_2$O$_3$	Methylene Blue	Visible; 10 ppm; 0,05 g; 100 min; 91,6%	(Alenad et al., 2023)
Ce/Co (Mo/Fe)	Methylene Blue	Visible; 20 ppm; 0,03 g; 120 min; 97,6%	(Ma et al., 2023)
Zinc Oxide	Methylene Blue	Visible; 5 ppm; 0,1 g; 120 min; 97%	(Bhapkar et al., 2023)
La/Ce-ZnO	Methylene Blue	Visible; 10 ppm; 0,1 g; 120 min; 95,2%	(Azmal et al., 2023)
Sn-CeO$_2$/TiO$_2$	Methylene Blue	Visible; 40 ppm; 0.2 g; 120 h; 85.5%	(Husna et al., 2023)
La$_2$O$_3$/TiO$_2$	Methylene Blue	Visible; 10 ppm; 0.25 g; 300 min; 87%	This result

CONCLUSIONS

The mixed oxide of TiO$_2$/La$_2$O$_3$ catalyst prepared by a simple method was used to degrade methylene blue dye under visible light conditions. The photocatalytic activity showed that the TiO$_2$/La$_2$O$_3$-923 (5) degraded methylene blue dye in visible light up to 94%. The bandgap energy of the TiO$_2$/La$_2$O$_3$-923 (5) is smaller than that of pristine TiO$_2$. However, the decrease in the bandgap energy is not a major factor in its photocatalyst activity. Two main factors are increasing the photocatalytic of TiO$_2$/La$_2$O$_3$-923, the presence of La$_2$O$_3$ on the surface of the photocatalyst that inhibits the recombination process, and the abundant -OH (*oop*) on the surface of the photocatalyst producing more hydroxyl radicals. The stability of the photocatalyst is high up to 3 sequent runs.

REFERENCES

Alenad, A. M., Suleman, M., Aman, S., Ahmad, N., Khan, R., Yasmin, R., & Taha, M. (2023). Visible light-driven Ni-doped hematite for photocatalytic reduction of noxious methylene blue. *Materials Research Bulletin*, *165*, 112306.

Alexander, J. T., Hai, F. I., & Al-aboud, T. M. (2012). Chemical coagulation-based processes for trace organic contaminant removal: Current state and future potential. *Journal of Environmental Management*, *111*, 195–207.

Aronne, A., Fantauzzi, M., Imparato, C., Atzei, D., De Stefano, L., D'Errico, G., & Rossi, A. (2017). Electronic properties of TiO$_2$-based materials characterized by high Ti^{3+} self-doping and low recombination rate of electron-hole pairs. *RSC Advances*, *7*(4), 2373–2381.

Ata, S., Shaheen, I., Aslam, H., Mohsin, I. U., Alwadai, N., Huwayz, M. Al, & Younas, U. (2023). Barium and strontium doped La-based perovskite synthesis via sol-gel route and photocatalytic activity evaluation for methylene blue. *Results in Physics*, *45*, 106235.

Awad, A. M., Shaikh, S. M. R., Jalab, R., Gulied, M. H., Nasser, M. S., Benamor, A., & Adham, S. (2019). Adsorption of organic pollutants by natural and modified clays: A comprehensive review. *Separation and Purification Technology*, *228*, 115719.

Azam, M. U., Tahir, M., Umer, M., Jaffar, M. M., & Nawawi, M. G. M. (2019). Engineering approach to enhance photocatalytic water splitting for dynamic H2 production using La$_2$O$_3$/TiO$_2$ nanocatalyst in a monolith photoreactor. *Applied Surface Science*, *484*, 1089–1101.

Azmal, Z. E. H., Sin, J.-C., Lam, S.-M., & Mohamed, A. R. (2024). Fabrication of La, Ce co-doped ZnO nanorods for improving photodegradation of methylene blue. *Journal of Rare Earths*, 42 (1), 76–83

Bai, C., Zhang, J. L., Hu, H. M., Wang, F., Wang, B. Z., Yan, L., & Wang, X. (2020). Influences of reaction temperature and pH on structural diversity of visible and near-infrared lanthanide coordination compounds based on bipyridyl carboxylate and oxalate ligands. *Journal of Solid State Chemistry*, *292*, 121691.

Bhapkar, A., Prasad, R., Jaspal, D., Shirolkar, M., Gheisari, K., & Bhame, S. (2023). Visible light-driven photocatalytic degradation of methylene blue by ZnO nanostructures synthesized by glycine nitrate auto combustion route. *Inorganic Chemistry Communications*, *148*, 110311.

Cao, G., Li, Y., Zhang, Q., & Wang, H. (2010). Synthesis and characterization of

La$_2$O$_3$@TiO$_2$−xFx and the visible light photocatalytic oxidation of 4-chlorophenol.pdf. *Journal of Hazardous Materials*, *178*, 440–449.

Colón, G., Hidalgo, M. C., & Navío, J. A. (2002). Effect of ZrO$_2$ incorporation and calcination temperature on the photocatalytic activity of commercial TiO$_2$ for salicylic acid and Cr(VI) photodegradation. *Applied Catalysis A: General*, *231*(1–2), 185–199.

Fleming, P., Farrell, R. A., Holmes, J. D., & Morris, M. A. (2010). The rapid formation of La(OH)$_3$ from La$_2$O$_3$ powders on exposure to water vapor. *Journal of the American Ceramic Society*, *93*(4), 1187–1194.

Herrmann, J. M. (2005). Heterogeneous photocatalysis: State of the art and present applications. *Topics in Catalysis*, *34*(1–4), 49–65.

Humayun, M., Raziq, F., Khan, A., & Luo, W. (2018). Modification strategies of TiO$_2$ for potential applications in photocatalysis: A critical review. *Green Chemistry Letters and Reviews*, *11*(2), 86–102.

Husna, R. A., Suherman, & Natsir, T. A. (2023). Enhancing photocatalytic degradation of methylene blue by mixed oxides TiO$_2$/ SnO$_2$ /CeO$_2$ under visible light. *Results in Engineering*, *19*, 101253.

Kustov, L. M., Borovkov, V. Y., & Kazansky, V. B. (1981). Spectra of hydroxyl groups in zeolites in the near-infrared region. *Journal of Catalysis*, *72*(1), 149–159.

Lan, Y., Lu, Y., & Ren, Z. (2013). Mini review on photocatalysis of titanium dioxide nanoparticles and their solar applications. *Nano Energy*, *2*(5), 1031–1045.

Le Page, Y., & Strobel, P. (1983). Structural chemistry of Magnéli phases Ti$_n$O$_{2n-1}$ (4 ≤ n ≤ 9). III. Valence ordering of titanium in Ti$_6$O$_{11}$ at 130 K. *Journal of Solid State Chemistry*, *47*(1), 6–15.

Li, H., & Feng, B. (2016). Visible-light-driven composite La$_2$O$_3$/TiO$_2$ nanotube arrays: Synthesis and improved photocatalytic activity. *Materials Science in Semiconductor Processing*, *43*, 55–59.

Liang, C. H., Li, F. B., Liu, C. S., Lü, J. L., & Wang, X. G. (2008). The enhancement of adsorption and photocatalytic activity of rare earth ions doped TiO$_2$ for the degradation of Orange I. *Dyes and Pigments*, *76*(2), 477–484.

Lin, J., & Yu, J. C. (1998). An investigation on photocatalytic activities of mixed TiO$_2$-rare earth oxides for the oxidation of acetone in air. *Journal of Photochemistry and Photobiology A: Chemistry*, *116*(1), 63–67.

Liu, T., Wang, L., Lu, X., Fan, J., Cai, X., Gao, B., & Lv, Y. (2017). Comparative study of the photocatalytic performance for the degradation of different dyes by ZnIn$_2$S$_4$: adsorption, active species, and pathways. *RSC Advances*, *7*(20), 12292–12300.

Ma, S., Shi, Y., Xia, X., Song, Q., & Yang, J. (2023). Cerium-cobalt bimetallic metal–organic frameworks with the mixed ligands for photocatalytic degradation of methylene blue. *Inorganic Chemistry Communications*, *152*, 110664.

Malato, S., Fernández-Ibáñez, P., Maldonado, M. I., Blanco, J., & Gernjak, W. (2009). Decontamination and disinfection of water by solar photocatalysis: Recent overview and trends. *Catalysis Today*, *147*(1), 1–59.

McManamon, C., O'Connell, J., Delaney, P., Rasappa, S., Holmes, J. D., & Morris, M. A. (2015). A facile route to synthesis of S-doped TiO$_2$ nanoparticles for photocatalytic activity. *Journal of Molecular Catalysis A: Chemical*, *406*, 51-57.

Moothedan, M., & Sherly, K. B. (2016). Synthesis, characterization and sorption studies of nano lanthanum oxide. *Journal of Water Process Engineering*, *9*, 29–37.

Natsir, T. A., Hara, T., Ichikuni, N., & Shimazu, S. (2018). Highly selective transfer hydrogenation of carbonyl compounds using La$_2$O$_3$. *Bulletin of the Chemical Society of Japan*, *91*(11), 1561–1569.

Obregón, S., & Colón, G. (2012). Evidence of upconversion luminescence contribution to the improved photoactivity of erbium doped TiO$_2$ systems. *Chemical Communications*, *48*(63), 7865–7867.

Pathania, D., Sharma, S., & Singh, P. (2017). Removal of methylene blue by adsorption onto activated carbon developed from Ficus carica bast. *Arabian Journal of Chemistry*, *10*, S1445–S1451.

Ranjit, K. T., Willner, I., Bossmann, S. H., & Braun, A. M. (2001). Lanthanide oxide-doped titanium dioxide photocatalysts: Novel photocatalysts for the enhanced degradation of p-chlorophenoxyacetic acid. *Environmental Science and Technology*, *35*(7), 1544–1549.

Tan, H., Zhang, Y., Li, B., Yang, H., Hou, H., & Huang, Q. (2023). Preparation of TiO$_2$-coated glass flat membrane and its photocatalytic degradation of methylene blue. *Ceramics International*, *49*(11), 17236–17244.

Wang, C. T., Chou, W. L., & Kuo, Y. M. (2009). Removal of COD from laundry wastewater by electrocoagulation/electroflotation. *Journal of Hazardous Materials*, *164*(1), 81–86.

Wang, R., Wang, F., An, S., Song, J., & Zhang, Y. (2015). Y/Eu co-doped TiO$_2$: Synthesis and photocatalytic activities under UV-light. *Journal of Rare Earths*, *33*(2), 154–159.

Wang, X., Jia, H., Wang, Y., Li, Y., & Bao, Z. (2016).

The photocatalytic performance research of La$_2$O$_3$ modified TiO$_2$ nanotube arrays. *Journal of Materials Science: Materials in Electronics*, *27*(7), 7073–7078.

Wu, H. H., Deng, L. X., Wang, S. R., Zhu, B. L., Huang, W. P., Wu, S. H., & Zhang, S. M. (2010). The preparation and characterization of La-doped TiO$_2$ nanotubes and their photocatalytic activity. *Journal of Dispersion Science and Technology*, *31*(10), 1311–1316.

Wu, H., Ma, J., Zhang, C., & He, H. (2014). Effect of TiO$_2$ calcination temperature on the photocatalytic oxidation of gaseous NH$_3$. *Journal of Environmental Sciences*, *26*(3), 673–682.

Xu, A. W., Gao, Y., & Liu, H. Q. (2002). The preparation, characterization, and their photocatalytic activities of rare-earth-doped TiO$_2$ nanoparticles. *Journal of Catalysis*, *207*(2), 151–157.

Xu, H., Li, H., Sun, G., Xia, J., Wu, C., Ye, Z., & Zhang, Q. (2010). Photocatalytic activity of La$_2$O$_3$-modified silver vanadates catalyst for Rhodamine B dye degradation under visible light irradiation. *Chemical Engineering Journal*, *160*(1), 33–41.

Yu, Y., Chen, G., Zhou, Y., & Han, Z. (2015). Recent advances in rare-earth elements modification of inorganic semiconductor-based photocatalysts for efficient solar energy conversion: A review. *Journal of Rare Earths*, *33*(5), 453–462.

Zhang, Y., Zhang, J., Xu, Q., Yan, S., Zhao, S., Luo, G., & Li, C. (2014). Surface phase of TiO$_2$ modified with La$_2$O$_3$ and its effect on the photocatalytic H$_2$ evolution. *Materials Research Bulletin*, *53*, 107–115.

Zhang, Z., Guo, Y., & Robertson, J. (2019). Atomic structure and band alignment at Al$_2$O$_3$/GaN, Sc$_2$O$_3$/GaN and La$_2$O$_3$/GaN interfaces: A first-principles study. *Microelectronic Engineering*, *216*, 111039.

Zhu, X., Pei, L., Zhu, R., Jiao, Y., Tang, R., & Feng, W. (2018). Preparation and characterization of Sn/La co-doped TiO$_2$ nanomaterials and their phase transformation and photocatalytic activity. *Scientific Reports*, *8*(1), 1–14.